Vectofusin-1, a potent peptidic enhancer of viral gene transfer forms pH-dependent α-helical nanofibrils, concentrating viral particles

Louic Vermeer, Loic Hamon, Alicia Schirer, Michel Schoup, Jérémie Cosette, Saliha Majdoul, David Pastre, Daniel Stockholm, Nathalie Holic, Petra Hellwig, et al.

Contents lists available at ScienceDirect

Acta Biomaterialia

journal homepage: www.elsevier.com

Full length article

Vectofusin-1, a potent peptidic enhancer of viral gene transfer forms pH-dependent α-helical nanofibrils, concentrating viral particles

Louic S. Vermeer[a], Loic Hamon[b], Alicia Schirer[c], Michel Schoup[a], Jérémie Cosette[d], Saliha Majdoul[e], David Pastré[b], Daniel Stockholm[e], Nathalie Holic[e], Petra Hellwig[c], Anne Galy[e], David Fenard[d, *, 1], Burkhard Bechinger[a, *]

[a] CNRS, Univ. of Strasbourg, Institut de Chimie UMR_7177, Strasbourg, France
[b] INSERM, Univ. of Evry, UMR_S1204, Evry, France
[c] CNRS, Univ. of Strasbourg, UMR 7140, Strasbourg, France
[d] Genethon, Evry, France
[e] Genethon, INSERM, Univ. of Evry, EPHE-PSL Research University, Research Unit Integrare UMR_S951, Evry, France

ARTICLE INFO

Article history:
Received 23 May 2017
Received in revised form 2 October 2017
Accepted 6 October 2017
Available online xxx

Keywords:
Lentiviral vector
Nanofibril
Amphipathic peptide
Gene therapy
Vectofusin-1

ABSTRACT

Gene transfer using lentiviral vectors has therapeutic applications spanning from monogenic and infectious diseases to cancer. Such gene therapy has to be improved by enhancing the levels of viral infection of target cells and/or reducing the amount of lentivirus for greater safety and reduced costs. Vectofusin-1, a recently developed cationic amphipathic peptide with a pronounced capacity to enhance such viral transduction, strongly promotes the entry of several retroviral pseudotypes into target cells when added to the culture medium. To clarify the molecular basis of its action the peptide was investigated on a molecular and a supramolecular level by a variety of biophysical approaches. We show that in culture medium vectofusin-1 rapidly forms complexes in the 10 nm range that further assemble into annular and extended nanofibrils. These associate with viral particles allowing them to be easily pelleted for optimal virus-cell interaction. Thioflavin T fluorescence, circular dichroism and infrared spectroscopies indicate that these fibrils have a unique α-helical structure whereas most other viral transduction enhancers form β-amyloid fibrils. A vectofusin-1 derivative (LAH2-A4) is inefficient in biological assays and does not form nanofibrils, suggesting that supramolecular assembly is essential for transduction enhancement. Our observations define vectofusin-1 as a member of a new class of α-helical enhancers of lentiviral infection. Its fibril formation is reversible which bears considerable advantages in handling the peptide in conditions well-adapted to Good Manufacturing Practices and scalable gene therapy protocols.

Abbreviations: AFM, atomic force microscopy; ATR-FTIR, attenuated total reflection Fourier transform infrared; CD, circular dichroism; DMEM, Dulbecco's modified eagle's medium; HPLC, high performance liquid chromatography; HSPC, hematopoietic stem/progenitor cells; LAH2-A4, peptide with the sequence KKALLAAALAALLALAHHLLALLKKA-NH2; LAH4-A4, peptide with the sequence KKALLHAALAHLLALAHHLLALLKKA-NH2; LV, lentiviral vector; MALDI-ToF, matrix-assisted laser desorption ionisation – time of flight; NMR, nuclear magnetic resonance; PBS, phosphate buffer saline; VF-1, vectofusin-1, another name for LAH4-A4; VSV-G, vesicular stomatitis virus envelope glycoprotein

* Corresponding authors at: Genethon, Technological Innovation Lentivirus, 1bis rue de l'Internationale, F-91000 Evry, France (D. Fenard). University of Strasbourg, Chemistry, 4 rue Blaise Pascal, F-67070 Strasbourg, France (B. Bechinger).
Email addresses: david.fenard@txcell.com (D. Fenard); bechinger@unistra.fr (B. Bechinger)
[1] Current address: TxCell SA, Allée de la Nertière, les Cardoulines, F-06560 Valbonne-Sophia Antipolis, France.

https://doi.org/10.1016/j.actbio.2017.10.009
1742-7061/

1. Introduction With the recent success in clinical trials using lentiviral vectors (LVs), gene therapy has seen a renaissance [1]. Its efficiency can be improved by enhancing transduction levels of target cells and its safety optimized by reducing the amount of viral vectors. One way to promote viral infectivity is the addition of culture additives such as the cationic polymer polybrene [2], a compound mainly used for laboratory research. The mechanism of action of this cationic additive is based on its ability to neutralize membrane charges and promote virus aggregation [3].

For clinical applications in gene therapy, transduction protocols include the polypeptide CH-296 (also called retronectin), a fragment of the human fibronectin [4–6]. Retronectin enhances transduction by promoting the co-localization of viruses and cells and rendering the target cell more permissive to the vector [7]. However, its use requires the surface coating of culture dishes which is not optimal both practically and for precise dosage of the additive relative to the vector. More importantly, retronectin is weakly efficient on the broadly used lentiviral vector pseudotyped with the vesicular stomatitis virus envelope glycoprotein (VSV-G-LV) [8,9]. Identification of new additives that are easy to manipulate and capable of enhancing the infectivity of a broad spectrum of LV pseudotypes is therefore required.

Peptide additives are interesting for their biodegradability, reduced size, simplicity of characterization (as compared to polymers), and the ease of production of a large range of different derivatives. In the last few years, new peptides with transduction enhancing activity have been identified and were shown to self-assemble into β-amyloid nanofibrils [10]. Examples of such peptides are the semen-derived enhancer of viral infection (SEVI) [11,12], the semenogelin peptides [13] or peptides derived from HIV-1 envelope glycoproteins, for example EF-C [14], P13 and P16 [15]. However, the formation of fibrils from semen-derived peptides is difficult (strong agitation of the peptide solution for days) and HIV-1 envelope-derived peptides are raising some concerns in terms of immunogenicity.

We recently focused our attention on the LAH4 peptide family, previously designed as antimicrobial agents while at the same time being efficient transfection agents for DNA and siRNA [16–22]. Some LAH4-derived peptides have been shown to strongly promote the transduction of human primary cells, especially hematopoietic stem/progenitor cells with various lentiviral pseudotypes, [23–25]. Furthermore, the lead peptide LAH4-A4, also called vectofusin-1 (VF-1), can be dosed to result in an infectivity of a single virus per cell, is not toxic on stem cells, and reduces the inoculum of viral vector needed by 2–3-fold, especially for the clinically used VSV-G-LV pseudotypes [24,25]. VF-1 promotes the adhesion and fusion between viral and cellular membranes [7,24]. Although the peptide has empirically shown to have many advantages over the other compounds used so far, the molecular basis of its mechanism of action and the reasons for its more favourable behaviour remain to be elucidated.

Here we investigated the VF-1 structure and its putative fibril formation as a function of environmental conditions by using thioflavin-T fluorescence, circular dichroism and infrared spectroscopies, as well as confocal, electron and atomic force microscopies. In contrast to the β-amyloid-like nanofibrillar arrangements by other peptides tested for viral transduction enhancement [10], VF-1 associates in a reversible manner from α-helical building blocks. The implications for the VF-1 mechanism of action and how these structural and biophysical insights can be used for the rational design of new transduction enhancing peptides are discussed.

2. Methods

2.1. Peptide synthesis

Vectofusin-1 (sequence: KKALLHAALAHLLALAHHLLALLKKA-NH_2) was synthesised with an amidated carboxy-terminus using a Millipore 9050 automated peptide synthesiser and standard Fmoc chemistry. The resulting product was purified by reverse-phase HPLC, and to exchange the trifluoroacetic acid counter ions washed three times with 4% (vol) acetic acid, freeze-dried, and stored at −18 °C. Its mass was verified by MALDI-ToF mass spectrometry and its purity confirmed by HPLC. For infrared spectroscopy, acetic acid counter ions were exchanged for chloride by three cycles of dissolving the peptide in a 10 mM HCl solution at a concentration of 1 mg/ml and lyophilisation. For some experiments (viral pull-down assay, AFM and confocal microscopy), VF-1 and LAH2-A4 (sequence: KKALL<u>A</u>AALA<u>A</u>LLALAHHLLALLKKA-NH_2, substituted amino acids underlined) were obtained from Genecust (Dudelange, Luxembourg) and used without further treatment.

.2.2. Viral vector production

Lentiviral vectors pseudotyped with the VSV-G envelope glycoprotein and encoding the modified nerve growth factor receptor marker (ΔNGFR) were labelled with the mCherry-Vpr fusion protein (VSV-G-mCherry-LV) and generated by transient calcium phosphate transfection of 293T cells with a 6-plasmid vector system as described previously [7] but using the pmCherry-Vpr plasmid [26]. Chromatography-purified VSV-G-LV particles encoding the enhanced green fluorescent protein (eGFP) were produced as described previously [27]. Infectious titres are expressed as the number of transduction units per millilitre (TU/ml) and physical titres as the number of p24 antigens per millilitre (ng p24/ml).

2.3. Viral pull-down assay

Chromatography-purified VSV-G-LV particles were diluted in culture medium to a final concentration of 100 ng p24/ml, and 500 µl of viral vectors were mixed with the indicated culture additive, homogenised, and centrifuged at 15,870 *g* for 10 min at room temperature. Supernatants were discarded and pellets suspended in 100 µl Dulbecco's modified Eagle's medium (DMEM, GIBCO Life Tech., St-Aubin, France). Viral pull-down efficiencies were evaluated by quantifying the p24 content in the pellets using a commercial HIV-1 p24 ELISA kit (Perkin Elmer, Courtaboeuf, France).

2.4. Thioflavin T assay

A stock solution of thioflavin T (Sigma Aldrich, St-Quentin-Fallavier, France) was prepared in phosphate buffer (10 mM Na_2HPO_4/NaH_2PO_4 + 150 mM NaCl at pH7) at 0.8 mg/ml, filtered and stored at −20 °C. The working solution was prepared extemporaneously by diluting (50x) in either water or X-Vivo20 medium (Lonza, Levallois-Perret, France). Subsequently, VF-1 (12 µg/ml) or EF-C (50 µg/ml) was incubated with thioflavin-T for the indicated amount of time. Fluorescence emission (excitation: 440 nm, emission: 482 nm) was recorded over time using a 2300Enspire spectrofluorometer (Perkin Elmer, Courtaboeuf, Les Ulis, France) and the baseline (buffer solution) was subtracted.

2.5. VF-1 imaging

Images of VF-1 solutions (1 mg/ml) in water, PBS 1x (Life Tech., St-Aubin, France) and X-Vivo20 medium were obtained with a Radiance scanning confocal system (Bio-Rad-Zeiss, Germany) mounted on a Nikon TE 300 microscope (Nikon Instech Co, Japan) with Nikon objectives (CFI S Fluor 40x oil). 2D movies or 3D reconstructions of confocal z-stack images were performed using the Image J software (Rasband, W.S., ImageJ, U. S. National Institutes of Health, Bethesda, Maryland, USA, http://rsbweb.nih.gov, 1997–2016).

Images of VF-1 fibrils (12 µg/ml) in contact with VSV-G-mCherry-LVs (6×10^5 TU/ml) were obtained with a scanning confocal microscope LEICA SP8 (Leica Microsystems, Germany). VF-1 (excitation: 488 nm, emission: 500–540 nm) and VSV-G-mCherry-LV emission (excitation: 552 nm, emission: 590–700 nm) were imaged with a 63x PL APO CS2 oil immersion objective 1.40 NA (Leica Microsystems, Germany). A z-stack was created by acquiring images every 0.4 µm. All images were deconvolved using Huygens Professional software (Scientific Volume Imaging, The Netherlands) before three-dimensional sample reconstruction. Finally, images were treated with a contrast enhancement algorithm (histogram equalization) and a 3-pixel radius median filter for background subtraction. For confocal images in presence of cells, HCT116 cells were cultured on Lab-Tek II Chamber Slide with cover (Lab-Tek, USA). LVs/VF-1 mix was added to cell culture for 1 h at 37 °C. Cells were then fixed with 1% PFA. The slide was mounted with Prolong Diamond with DAPI (Thermofisher, France) and using grade #1.5 24 mm × 50 mm coverslip (Dominique Dutscher, France). Images were then acquired. The DAPI channel (excitation: 405 nm, emission: 415–470 nm) was added to the optic configuration described previously and images were treated with the same contrast enhancement algorithm.

Emission spectra (ex. 488 nm) of VF-1 fibrils were acquired using a multimodal plate reader spectrofluorometer (2300Enspire) and the turbidity of the VF-1 solutions was evaluated by measuring the absorbance at 600 nm with a KC4 spectrophotometer (BioTek Instruments, St Quentin-en-Yvelines, France).

2.6. Atomic force microscopy (AFM)

Vectofusin-1 (1 mg/ml) was incubated at room temperature in DMEM culture medium. After incubation times ranging from 3 min to 1 day, the solution was diluted in DMEM culture medium to obtain a final VF-1 or LAH2-A4 peptide concentration of 10 µg/mL. A 10 µL droplet was deposited on a freshly cleaved mica surface and left to interact for 30 s. The mica surface was then rinsed with 0.02% uranyl acetate solution and dried with filter paper. AFM images recorded in air were acquired with a Nanoscope V Multimode 8 microscope (Bruker, Santa Barbara, CA, USA) in PeakForce Tapping mode using Scanasyst-Air-HR probes (Bruker). Images were recorded at 1024 × 1024 pixels at a line rate of 3 Hz for Fig. 3A, B, C; and at 3072 × 3072 pixels at 1.5 Hz for Fig. 3D.

2.7. AFM image analysis and statistical methods

The "particle analysis" tool on the Nanoscope Analysis software (version 1.50) was used to determine the diameter of 50 annular structures (Fig. 3B), for each incubation time and from at least three independent samples [28]. Filamentous structures, aggregates or structures of which the contours could not be determined were excluded from this analysis. The "section" tool on the same software was used to determine the height and periodicity along the fibril axis. Significance of diameter measurements were obtained using *t*-test; *, $p < .05$; **, $p < .01$; ***, $p < .005$; ns, not significant.

2.8. Transmission electron microscopy

For transmission electron microscopy, a solution of 5 mg/ml (1.6 mM) vectofusin-1 in 10 mM sodium phosphate at pH 4 or pH 8 was deposited on a carbon grid. After 2 min the excess sample was removed with filter paper and a solution of filtered (0.22 µm) ammonium molybdate (1% w/v) at pH 4 or pH 8 was added and left to interact for 2 min prior to the removal of excess solution with filter paper. TEM images were recorded with an AMT Hamamatsu digital camera (Advanced Microscopy Techniques, Woburn, MA, USA) on a Hitachi (Krefeld, Germany) H-7500 electron microscope at 80 kV.

2.9. Circular dichroism (CD) spectroscopy

A stock solution of 1 mg/ml (0.3 mM) in 10 mM sodium phosphate at pH 4.3 was prepared and diluted 10 times with 10 mM sodium phosphate. Throughout the manuscript we use the term "phosphate" to cover both the $H_2PO_4^-$ and the HPO_4^{2-} ions. With a phosphate pKa of 7.2, the ionisation state can be deduced from the context. From a stock solution of 2–3 µl, 0.5 M NaOH was added to increase the pH in a stepwise manner and a CD spectrum was recorded using a quartz cuvette with a path length of 1 mm on a Jasco J-810 spectrometer (Jasco, Tokyo, Japan) at 25 °C, with wavelengths between 260 and 190 nm in steps of 1 nm with a stepping speed of 50 nm/min. Baselines of samples without peptide were subtracted and except for summing the 10 scans acquired for each spectrum and conversion from machine units to mean residual ellipticity ($deg\,cm^2\,dmol^{-1}$), no spectral processing was carried out.

2.10. Attenuated total reflection Fourier transformed infrared (ATR-FTIR) spectroscopy

ATR-FTIR analyses were performed on a Bruker Vertex 70 FTIR spectrometer (Karlsruhe Germany) equipped with a Harrick-Diamond ATR. 3 µL of a solution of 20 mg/ml (6.6 mM) vectofusin-1 in D_2O (Sigma-Aldrich, 99,9% purity) or 20 mM sodium phosphate in D_2O at pH 4 or pH 8 were deposited on the diamond plate and dried under an argon flow. Infrared spectra were recorded in the 4000–700 cm^{-1} spectral range with a resolution of 4 cm^{-1} and 256 scans co-added.

2.11. Statistical considerations associated with CD- and ATR-FTIR spectra

To analyse the structural changes as a function of lipid concentration or pH only spectral changes that are significantly more pronounced than the noise level were taken into consideration. Notably, whereas considerable errors can occur during the deconvolution of CD- and FTIR spectra [29] here we performed a semi-quantitative analysis and/or followed the relative changes in spectral intensities during titration experiments.

3. Results

3.1. Vectofusin-1 forms peptide aggregates that sediment viral particles

VF-1 stock solutions are soluble in water (pH < 6) at concentrations around 1–5 mg/ml, but the solution becomes turbid when suspended in phosphate buffered saline (PBS). In X-vivo20 culture

medium, used in clinical settings for viral transduction of hematopoietic stem cells, macroscopic aggregates are formed (Fig. 1A-B). Interestingly, these VF-1 aggregates can be observed because of their photoluminescence (Fig. 1C), with an emission peak around 518 nm (Fig. 1D). A dense network of small aggregates is observed in PBS and large aggregates in X-vivo20 medium (Fig. 1C and Supplemental videos). To characterise the network of VF-1 fibrils formed in stock solution (5 mg/ml), electron microscopy images were acquired in phosphate at pH 4 and pH 8 (below and above the pKa of histidine). At pH 4, no supramolecular aggregate formation was observed (not shown), while at pH 8 a dense network of fibrils is visible (Fig. 1E).

Numerous known viral transduction enhancers self-assemble in supramolecular structures capable of trapping viral particles [10]. This feature can be evaluated using a viral pull-down assay, as described previously for the EF-C or SEVI fibrils [14,30]. Whereas the biological efficiency of VF-1 has been compared to retronectin and SEVI in previous publications [23,24] here we included EF-C another highly efficient enhancer peptide for viral transduction. Notably by centrifugation alone viruses remain in solution and cannot be analysed. As shown in Fig. 2A, VF-1 promotes the sedimentation of 46% to nearly 100% of viral particles at concentrations typically used in biological settings (12–24 µg/ml corresponding to 4.3–8.6 µM) being as efficient as EF-C. To observe the complex between VF-1 peptide aggregates and lentiviral particles, the latter were labelled with mCherry fluorescent proteins (VSV-G-mCherry-LVs), incubated with VF-1 aggregates, and sedimented by centrifugation. Images of the resulting fibril-virion complexes obtained by deconvoluted confocal microscopy are shown in Fig. 2B, and confirm the association of viral particles with a network of VF-1 aggregates. When mixtures of VF-1 and LVs were added to HCT116 cells, some VF-1/LV complexes seem to co-localize with the cell surfaces but the intense autofluorescence at the same frequency of both cells and VF-1 elongated aggregates make the exact delineation of these structures difficult (Fig. S1).

3.2. Vectofusin-1 peptides self-assemble as nanofibrils

To study the nature of the VF-1 aggregates in further detail, they were visualized using atomic force microscopy at the concentration optimal for viral transduction (10 µg/ml, i.e. 500-fold less concentrated than the EM image shown in Fig. 1E). Images show isolated as well as clustered nanostructures with a spherical appearance (Fig. 3). Interestingly, those structures associate over time in annular and linear arrangements (Fig. 3A-C) with a periodicity of 10 nm (Fig. 3D). The diameters of the annular structures increase upon the first minutes of incubation (Fig. 3B). Their height profiles are dominated by a 3 nm population with a smaller fraction measuring 4.5 nm (Fig. 3C) and some scatter at 5–12 nm. At later time points, extended linear structures are observed. A variant of VF-1 that lacks two critical histidine residues (LAH2-A4) (Fig. 4A), does not promote lentiviral transduction [25]. No supramolecular structures were observed for this inactive peptide (Fig. 4C), suggesting that larger molecular peptide assemblies are required for transduction enhancement. This is in line with the lack of viral pull-down efficiency by LAH2-A4 (Fig. 4D).

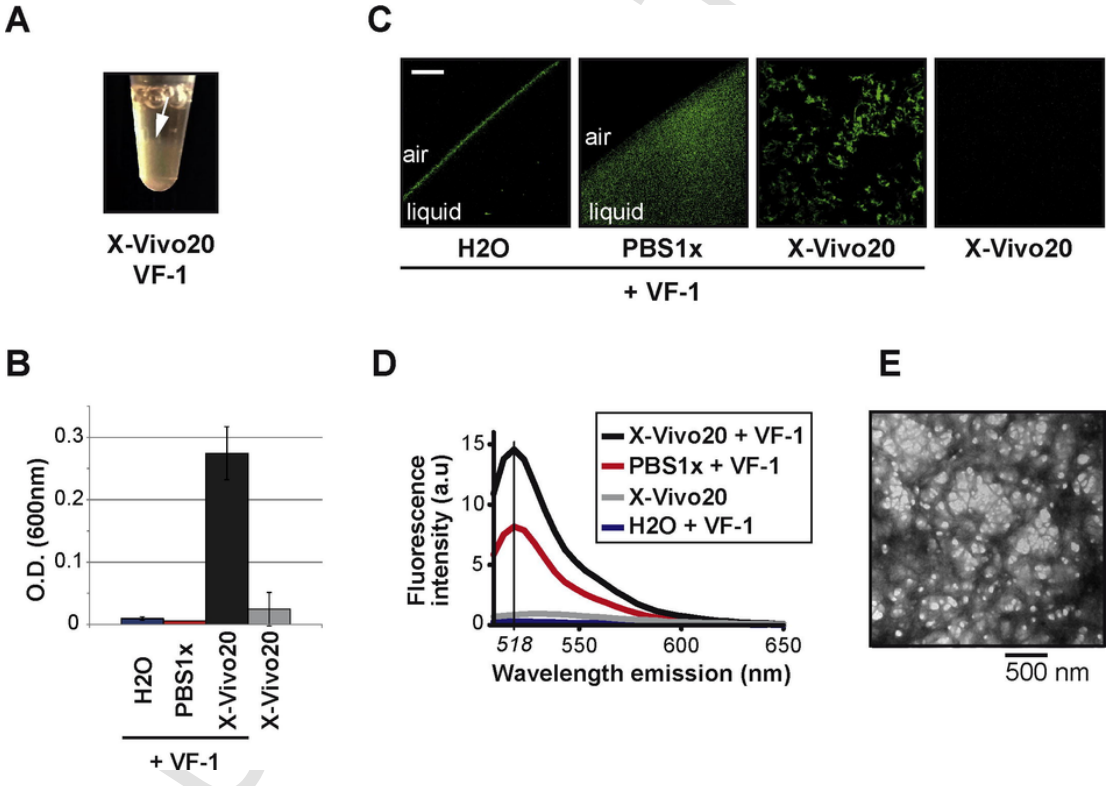

Fig. 1. Vectofusin-1 forms aggregates in phosphate buffer and in culture medium. (A) A VF-1 solution (1 mg/ml) 30 min after suspension in X-Vivo20 medium (the arrow is pointing at the interface of sedimented VF-1 fibrils). (B) Optical density (600-nm) of VF-1 solutions, where the error bars represent the standard deviation of three independent experiments. (C) Confocal microscopy of VF-1 (1 mg/ml) suspended in H_2O, PBS 1x or X-Vivo20 medium (Scale bar, 1 µm). Images in H_2O and PBS 1x were taken to cross-section the air/water interface of the VF-1 solution droplet. (D) Emission spectra (ex. 488 nm) of the VF-1 solutions/suspensions observed in C. (E) Negatively stained transmission electron microscopy image (80 kV, 50000x magnification) of 5 mg/ml VF-1 peptides in 10 mM phosphate buffer at pH 8.

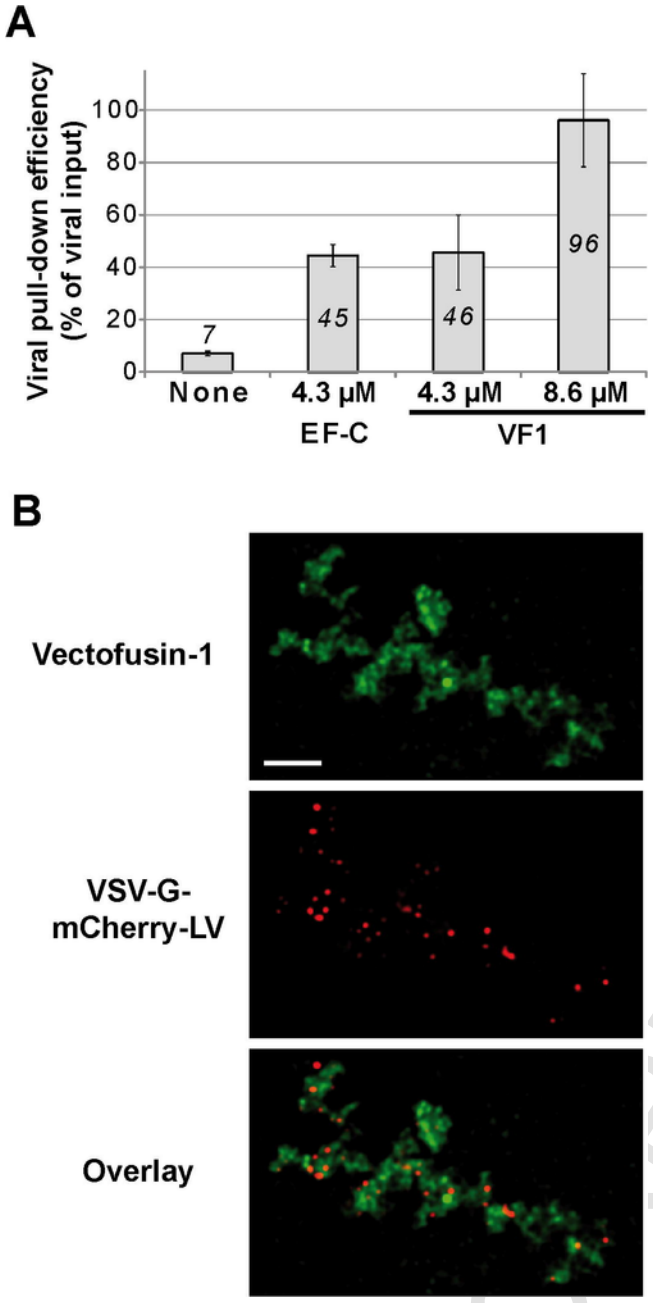

Fig. 2. Vectofusin-1 fibrils co-localise with viral particles. (A) VSV-G-LVs were mixed with EF-C or VF-1 peptides at indicated concentrations. After a low speed centrifugation, the HIV-1 p24 antigen content in the pellet was evaluated by an ELISA assay and represented as percentage of viral pull-down normalized to the viral input ± SEM (n = 5). (B) Confocal microscopy of VF-1 fibrils in contact with VSV-G-mCherry-LVs (scale bar 3 µm). The centrifugation step was performed within a few minutes after mixing the compounds.

3.3. The vectofusin-1 nanofibrils have α-helical structure

To further investigate the structure of these nanofibrils and their pH dependence, a pH titration by circular dichroism (CD) spectroscopy was carried out. Fig. 5A shows that VF-1 is unstructured at low pH and adopts an α-helical structure above pH 6.1. An isodichroic point at 205 nm is observed, confirming a two-state transition from unstructured to α-helical. So far, the observed behaviour is similar to many other cationic amphipathic peptides such as LAH [31], LAK, LAO [32], and LADap peptides [33] that are used for nucleic acid delivery or as antimicrobials. Notably, for VF-1, the ratio of molar ellipticities at 222 nm and 208 nm ($\theta_{222}/\theta_{208}$) is >1.0, indicative of helix association [34]. The helix formation precedes the formation of larger self-associated complexes: above pH 6.1 the spectra no longer pass through the isodichroic point at 205 nm, but a new isodichroic point at 200 nm appears. Fig. 5B shows the ellipticity per residue as function of pH at each of the isodichroic points. Curve fitting estimates the pKc values of these conformational transitions at 5.5 and 6.7. Although the titration shown here was started at low pH, the reverse titration gives the same results and thus indicates that the peptide self-association is reversible.

Interactions of bivalent ions have been found important for the assembly of some β-amyloids [35], cationic polymers [36] or the packing of peptide oligomers [37]. In order to define the role of phosphates for the VF-1 supramolecular structures, the peptide in water was titrated with increasing phosphate concentrations at pH 4.6 and 7.4 (Supplementary Figs. S2 and S3). At pH 4.6, VF-1 remains unstructured after addition of 5.3 mM phosphate (160 phosphate ions per peptide), even after 10 days at room temperature. At pH 7.4, no change in the α-helical structure was detected up to phosphate concentrations of 2.4 mM (66 phosphates per peptide), but at 4 mM (111 per peptide) a phosphate-induced increase in the ratio of molar ellipticities at 222 nm and 208 nm ($\theta_{222}/\theta_{208}$) was observed (Fig. S3), which has been taken as an indicator for oligomeric coiled-coil structures [34].

To the best of our knowledge, all the short peptides with viral transduction enhancing activities form amyloid β-sheets [10]. In contrast, our structural investigations by CD spectroscopy show that VF-1 occurs either as an unstructured peptide at low pH or as an α-helix under biological conditions, while the CD spectra of EF-C β-sheet nanofibrils exhibit different features (SI of [14]). Since circular dichroism is known to be more sensitive to α-helical structures, attenuated total reflection Fourier transform infrared spectroscopy (ATR-FTIR) was used as a complementary technique, known to be more prone to reveal β-sheets. Spectra were recorded in D_2O in absence or presence of 20 mM phosphate. At pH 4.0, a non-viscous solution was obtained, but at pH 8.0 a transparent, viscous gel formed in the tube. This gel was deposited on the crystal. The amide I region of the processed spectrum is shown in Fig. 6A. In all conditions tested, the spectral profile of VF-1 is clearly different from the designed amyloid peptides [38,39] and transduction enhancing EF-C β-sheet nanofibrils [14], that exhibit typical and predominant features at 1695–1672 cm^{-1} and 1638–1615 cm^{-1} [40]. A comparison of IR spectra recorded from β-sheet and VF-1 nanofibrils is shown in Fig. S4. These spectroscopic data are further confirmed by the absence of thioflavin T fluorescence in presence of VF-1 (Fig. 6B), an assay thought to specifically label β-amyloids [41] such as EF-C. Although CD spectroscopy suggests the presence of unstructured peptide at low pH, no random coil signal at 1670 cm^{-1} is detected: the higher concentration and the drying of the peptide on the crystal induce the self-association even at low pH. Taken together, the IR peak position near 1650 cm^{-1}, the lineshape of the circular dichroism spectra and the lack of thioflavin-T fluorescence indicate that VF-1 forms α-helical coiled-coil fibrils at physiological pH.

4. Discussion

VF-1 has been described as a strong enhancer of viral transduction, acting on the adhesion and fusion steps of lentiviruses developed for gene therapy [7,24,25]. In this manuscript, we show that this

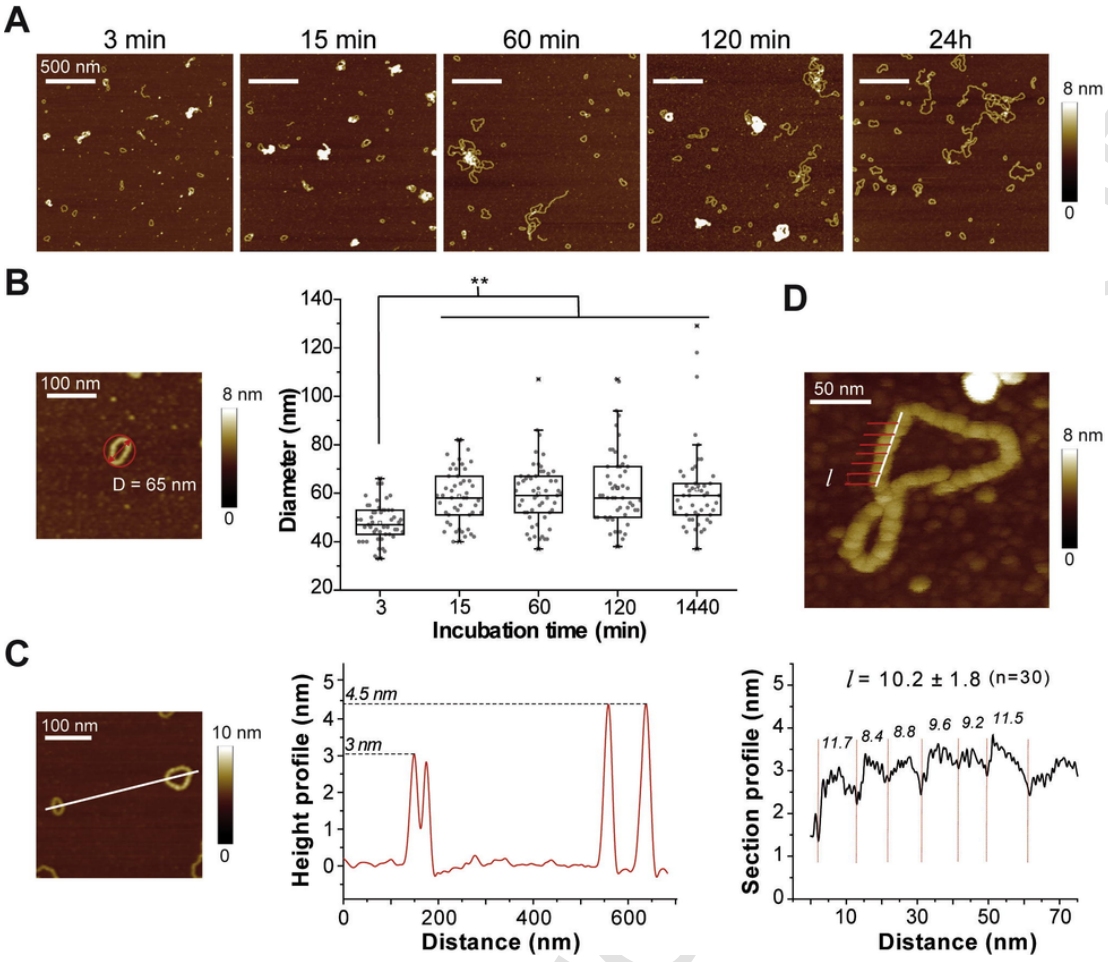

Fig. 3. AFM shows vectofusin-1 self-assembly as annular and linear structures. (A) VF-1 peptides were incubated at 1 mg/ml in DMEM culture medium for the indicated times and diluted to 10 µg/ml. Annular and linear structures were detected on the mica surface (scale bar 500 nm, Z-scale 8 nm). (B) AFM image (left panel) of an annular structure describing how diameters (here 65 nm, red circle) were measured and box plot of the diameters of annular structures measured in AFM images as a function of incubation time. The boxes (25–75 percentiles), vertical bars (5–95 percentiles) and data points (circles, n = 50 particles) are shown in relation to the mean value (empty square) and median value (horizontal line in the box). **p < .01, *p < .05, two-tailed *t* test. (C) On the right panel, height profiles of two annular structures corresponding to the AFM image on the left. (D) High resolution observations (upper panel) indicate a periodicity of approximately 10 nm along the fibril axis (white line), shown in the lower panel (n = 30). (For interpretation of the references to colour in this figure legend, the reader is referred to the web version of this article.)

peptide forms supramolecular assemblies that co-localize with lentiviral particles (Fig. 2), leading to sedimentation and thus increasing local virus concentrations along the cellular surface of target cells. It may also be expected that virus-cell adhesion is increased because the positively charged peptides reduce the electrostatic repulsion between negatively charged membranes without compromising the viral envelope and cellular membrane integrity [3]. Notably, fibre formation and viral pull-down activity are absent for LAH2-A4, a closely related VF-1 derivative lacking transduction enhancement activities, suggesting that fibril formation and the resulting co-localization of lentiviruses with such VF-1 supramolecular assemblies are important for this activity [10]. In this regard, VF-1 is related to other known viral transduction enhancers that self-assemble in supramolecular structures capable of trapping viral particles [10] such as semen-derived peptides and HIV-1 derived peptides, which enhance transduction by promoting the co-localization of viruses and cells [7]. But in contrast to these peptides, VF-1 is not requiring a strong agitation during hours to form fibrils since VF-1 supramolecular assembly occurs spontaneously in culture medium [24,25].

Using atomic force microscopy we have demonstrated at the nanoscale level that VF-1 self-associates into supramolecular complexes with spherical appearance in AFM images, that further assemble into fibrils with an annular or a spiral turn appearance (Fig. 3). Within hours these convert into longer fibrils. The formation of annular protofibrils and fibril elongations has been extensively described in preparations of different amyloidogenic proteins and peptides [42–45]. Interestingly, most of the short peptides with viral transduction enhancing activities form amyloid β-sheets [10], including SEVI [11,12], the semenogelin peptides [13], EF-C [14], P13 and P16 [15].

To better understand the molecular interactions that lead to such supramolecular assemblies, comparison with previously described helical coiled-coil fibrils from natural sources or by design is helpful. Helical coiled-coils are abundant in proteins [46,47] and some fibrils derived from *α*-helical coiled-coil motifs have been described in native biological systems [48]. Whereas the transition from random coil to helical has been observed for cationic amphipathic peptides with nucleic acid delivery or antimicrobial activities, including LAH [31], LAK, LAO [32], LADap peptides [33] or magainins [49], the design of α-helical peptides for creating synthetic biomaterials, a relatively recent topic, has initially proven to be complex but has taken up speed [50,51]. In a first step, much effort went into the design of coiled-coil building blocks of defined oligomeric size where hy-

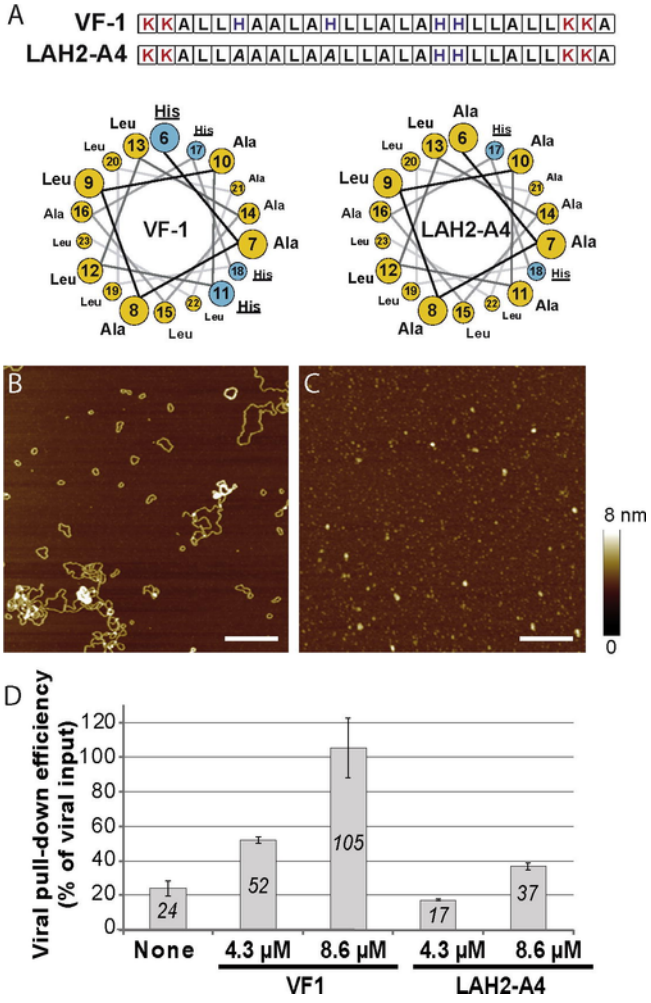

Fig. 4. The VF-1 histidine mutant LAH2-A4 is unable to form nanofibers and sediment viral particles. (A) Schiffer-Edmundson helical wheel diagrams of VF-1 and of LAH2-A4. Amino acid residues 4–23 are shown. Atomic Force Microscopy after 60 min of incubation of 1 mg/ml peptide in DMEM and dilution to 10 µg/ml shows fibril formation by VF-1 (B) but not by LAH2-A4 (C) (scale bars 400 nm, Z-scale 8 nm). (D) Viral pull-down assay. VSV-G-LVs were mixed with VF-1 or LAH2-A4 peptides, respectively, at the indicated concentrations. After a low speed centrifugation, the HIV-1 p24 antigen content in the pellet was evaluated by an ELISA assay and represented as percentage of viral pull-down normalized to the viral input ± SD (n = 2).

drophobic interactions, electrostatic repulsion and attraction are carefully tuned [52]. In a next step, order along the long axis of the fibre was introduced which usually involved much longer peptides. For example, contacts in the longitudinal direction were based on a staggered 5-heptat repeat where pH dependence arises from arginine and glutamate residues [53,54]. Alternatively, 'sticky ends' were created by overhanging coiled-coil dimers from two different peptides with complementary charge [55], as well as blunt end [39] or lock-washer interfaces which associate by charge complementarity [52]. Furthermore, repulsive electrostatic forces at the polar faces of the coiled-coil ensured that lateral aggregation does not interfere with longitudinal order [52]. Based on such features, α-helical coiled-coil sequences were designed *de novo* that, in a pH-dependent manner, form either fibrils or spherical particles [54]. In contrast, VF-1 does not contain negative charges: an amidated C-terminus and the presence of four lysine residues give it a net charge of +5 at neutral pH, and four histidine residues increase this to +9 at a pH below 6. Considerable ingenuity was required to design α-helical peptide sequences that self-assemble into fibrous structures [50,51]. Therefore, the question arises how VF-1 self-associates into extended fibrils and meshes. The amino acid sequence and comparison to previously published principles, some discussed above, provide some clues for speculation.

While the supramolecular arrangement within VF-1 fibrils remains unknown, a height of about 3.5–4.5 nm and a periodicity along the fibril axis of ~10 nm (Fig. 3) suggest the involvement of multiple peptides (Fig. S5). Dimensions of a coiled-coiled dimer are 2 nm [56] and increase only slowly when more helices bundle up [52–54]. The CD ratio of molar ellipticities at 222 nm and 208 nm ($\theta_{222}/\theta_{208}$) > 1.0 has been shown to be an indicator of interfacial helix association and the formation of coiled-coil structures [34,57]. Indeed, the presence of multiple leucine residues in the hydrophobic core and their localization on one face of the α-helix (Fig. 4) agrees with the formation of a building block based on leucine-zipper-like interactions [25], where the knobs-into-holes complementarity allows for lateral packing [46,47]. Hydrophobic residues not involved in the zipper could promote longitudinal self-association. The opposite polar face of VF-1 consists of alanine and histidine residues, where the inactive LAH2-A4 [25] has its first two histidine residues replaced with alanine (Fig. 4). The fact that the latter does not form fibrils indicates that those histidine residues are essential for the fibril formation and thus play an important role in intermolecular interactions. Our structural investigations show that VF-1 is highly soluble and unstructured at acidic pH while it rapidly adopts an α-helical conformation above pH 6 and assembles further into coiled-coil structures at the neutral pH used during viral transduction (Figs. 5 and 6). This strengthens the hypothesis of the involvement of histidine (pKa ~6), and further suggests that the imidazole side chains need to be in their deprotonated, uncharged state for fibril formation to occur. Replacement of histidine with alanine prevents the association into large supramolecular structures (Fig. 4C), indicating that the removal of repulsive Coulombic interactions alone is not sufficient for fibril formation at neutral pH. A deprotonated histidine sidechain is a hydrogen bond acceptor and can participate in π-π stacking or cation-π interactions. Previous studies have indeed shown that His-His interactions are stronger when histidine is deprotonated [58], and that such interactions are quite common in proteins [59]. However, based on the current data, we cannot exclude that interactions between histidine and either lysine, the terminal carboxyamide or the amino-terminus are involved in the self-association.

To make matters even more complex, phosphate buffer was found to promote self-association of α-helical VF-1 even at low ionic strength (Supplementary Figs. S2 and S3). The pH-dependent structural transition of VF-1 shows pKc values of 5.5 and 6.7 (Fig. 5). With the typical histidine pKa being 6.2 in solution and phosphate having a theoretical pKa of 7.2, the pKc of 5.5 seems linked to the (de)protonation of the histidine side chains and the pKc of 6.7 is suggestive that the equilibrium between $H_2PO_4^-$ and $H_2PO_4^{2-}$ from the buffer is involved in the structural transition of VF-1, similar to the involvement of bivalent ions in the formation of some β-amyloids [35], cationic polymers [36] or the packing of peptide oligomers [37]. It is well possible that the histidine pKa is reduced, favouring the uncharged state, by conformational changes that increase Coulombic interactions with nearby positive charges [60] and/or insertion in a more hydrophobic environment [61], for example due to the observed peptide self-association. An important role of phosphates has been described for β-amyloids of β-endorphin [35], a contraction of polylysine polymers has been reported due to the electrostatic interactions of bivalent phosphate and the cationic lysine side chains [36] and phosphate ions have been found important in the packing of a homodimer antimicrobial peptide [37], suggesting that phosphate or

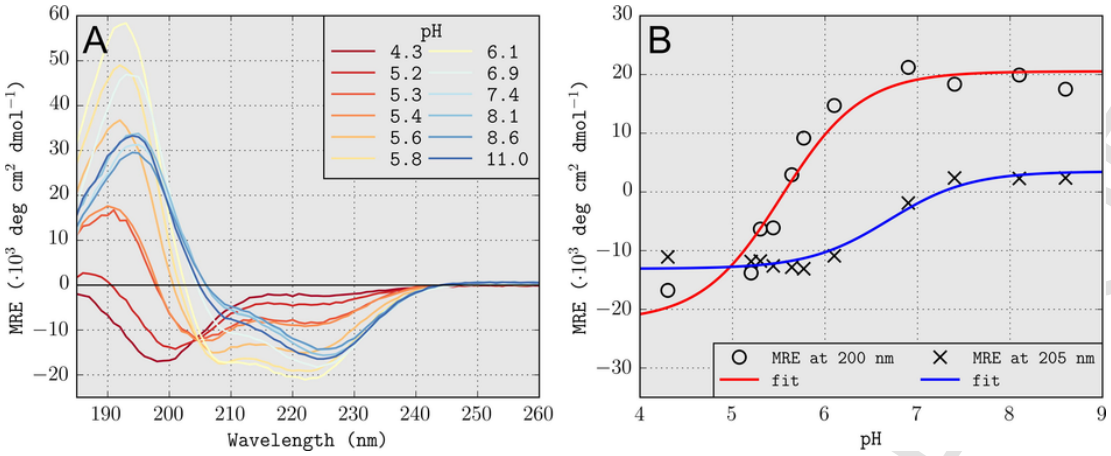

Fig. 5. Secondary structure analysis of VF-1 suspensions by circular dichroism spectroscopy after one day of incubation on the bench. (A) pH titration of VF-1 in 10 mM phosphate. (B) The two steps of fibril assembly as viewed by CD spectroscopy. The mean ellipticity per amino acid residue is plotted at the wavelengths of the two isodichroic points observed in panel A and fitted with sigmoidal curves to determine the characteristic pKc values of the structural transitions: 5.5 and 6.7.

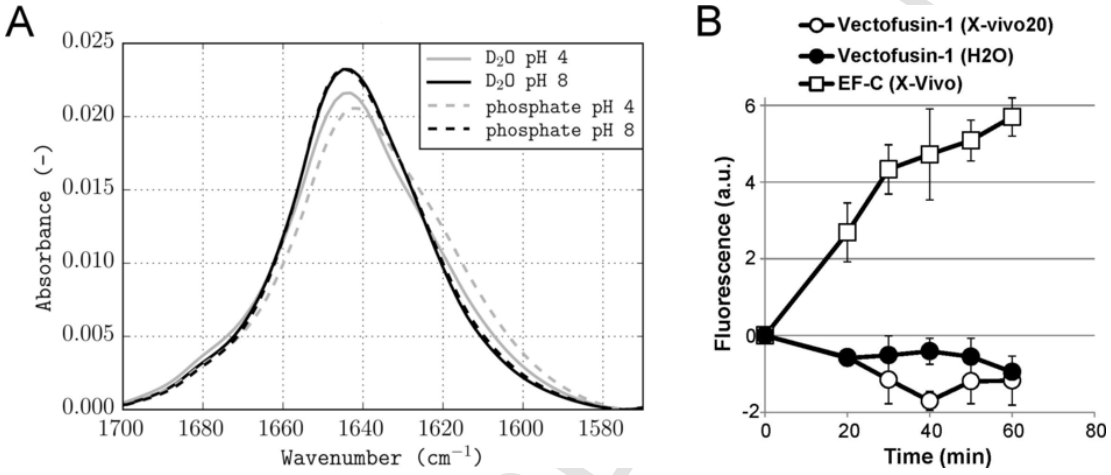

Fig. 6. ATR FT-IR and Thioflavin-T fluorescence show no evidence for the presence of β-sheet structures in VF-1. (A) The amide I region of ATR-FTIR spectra of VF-1 recorded in D_2O only (solid lines) or D_2O in presence of 20 mM phosphate (dotted lines), at pH 4 (grey) or pH 8 (black). The sample was applied to the diamond plate after a 6.6 mM VF-1 solution has been incubated for a few hours of incubation on the bench. Depending on the pH, the term "phosphate" in the legend refers to either predominantly $H_2PO_4^-$ or HPO_4^{2-}. (B) A thioflavin T stock solution was diluted either in water (black) or in X-vivo20 medium (white) to a final concentration of 16 μg/ml and incubated with 12 μg/ml VF-1 (circles) or 50 μg/ml EF-C peptide (squares) for the indicated amount of time. The fluorescence intensity (ex. 440 nm, em. 482 nm) was recorded and background without peptide subtracted. Data are representative of three different experiments performed in triplicate ± SD.

other anions have a structural role during the VF-1 association process. Additional high-resolution structural investigations are in progress to better define the molecular interactions involved in the self-assembly of VF-1.

5. Conclusion

The viral transduction enhancing peptide VF-1 belongs to a novel class of α-helical fibril-forming transduction enhancers and has not shown any propensity for amyloid formation in our experiments. To the best of our knowledge, that makes VF-1 the first transduction enhancing peptide that forms α-helical coiled-coil fibrils instead of amyloid β-sheets [10]. It is of interest that some β-sheet nanofibers or their precursors are associated with pathologies [62], whereas the use of coiled-coil α-helical materials has so far not been a concern. The VF-1 assembles into long fibrils composed of multiple spherical particles with a diameter around 10 nm. They form fibrils that appear to close back on themselves giving them an annular appearance, which is lost during the elongation that takes place on a timescale of hours under the conditions used for gene therapy transduction protocols. The pH dependence and reversibility of this fibril formation bears considerable advantages in handling the peptide under conditions well-adapted to Good Manufacturing Practices and scalable gene therapy protocols using lentiviral vectors in which, at present, the cumbersome retronectin additive is typically used. VF-1 peptides can be stored and dosed precisely from a stock solution at low pH and/or the absence of phosphate and subsequently diluted in culture medium at physiological pH to ensure fibril formation in presence of lentiviral vectors and before addition to the cell suspension. In conclusion, the family of histidine-rich LAH4 peptides bears considerable promise for LV transduction, in particular in clinical settings where the rational design of pH-sensitive self-associating α-helical peptides can contribute to further improvements of gene therapy treatments.

Notes

The authors declare no competing financial interest.

Acknowledgments

We are most grateful to Christopher Aisenbrey for the simulations of the beta-contributions of the EF-C IR spectrum and his advice with peptide synthesis. The authors thank Delphine Hatey for helping with peptide synthesis and purification, Valérie Demais, Cathy Royer and Frank Pfrieger for the electron microscopy, and Genethon collaborators, especially Ababacar Seye and Antoine Gachet for technical assistance. We also acknowledge Hugues de Rocquigny for the kind gift of pmCherry-Vpr plasmid.

This work was supported by the Fondation pour la Recherche Médicale (FRM) [grant number DCM2012-1225742], awarded to AG, BB and DF, as well as the Association Française contre les Myopathies (AFM), the FRR award from the University of Evry awarded to DF. Additionally, the financial contributions to BB's team of the Agence Nationale de la Recherche [TRANSPEP 07-PCV-0018 and LabEx Chemistry of Complex Systems 10-LABX-0026_CSC] are gratefully acknowledged, as well as financial contributions from the University of Strasbourg, CNRS, Région Grand–Est (Alsace) and the RTRA International Center of Frontier Research in Chemistry. DP and LH gratefully acknowledge the Institut National de la Santé et de la Recherche Médicale, the Agence Nationale de Recherches sur le Sida (ANRS, grant number N1409OJR) and the Genopole Evry for constant support of the laboratory. Last but not least, BB is grateful to the Institut Universitaire de France for providing additional time to be dedicated to research.

Appendix A. Supplementary data

Confocal Microscopy movies of VF-1 aggregates, image of VF-1/LV complexes in cell culture, phosphate titration of VF-1 by CD-spectroscopy, comparison of FTIR spectra and size comparison of helical peptides and fiber dimensions. Supplementary data associated with this article can be found, in the online version, at https://doi.org/10.1016/j.actbio.2017.10.009.

References

[1] L. Naldini, Gene therapy returns to centre stage, Nature 526 (7573) (2015) 351–360.
[2] K. Toyoshima, P.K. Vogt, Enhancement and inhibition of avian sarcoma viruses by polycations and polyanions, Virology 38 (3) (1969) 414–426.
[3] H.E. Davis, M. Rosinski, J.R. Morgan, M.L. Yarmush, Charged polymers modulate retrovirus transduction via membrane charge neutralization and virus aggregation, Biophys. J. 86 (2) (2004) 1234–1242.
[4] T. Moritz, V.P. Patel, D.A. Williams, Bone marrow extracellular matrix molecules improve gene transfer into human hematopoietic cells via retroviral vectors, J. Clin. Invest. 93 (4) (1994) 1451–1457.
[5] T. Moritz, P. Dutt, X. Xiao, D. Carstanjen, T. Vik, H. Hanenberg, D.A. Williams, Fibronectin improves transduction of reconstituting hematopoietic stem cells by retroviral vectors: evidence of direct viral binding to chymotryptic carboxy-terminal fragments, Blood 88 (3) (1996) 855–862.
[6] H. Hanenberg, X.L. Xiao, D. Dilloo, K. Hashino, I. Kato, D.A. Williams, Colocalization of retrovirus and target cells on specific fibronectin fragments increases genetic transduction of mammalian cells, Nat. Med. 2 (8) (1996) 876–882.
[7] D. Ingrao, S. Majdoul, A.K. Seye, A. Galy, D. Fenard, Concurrent measures of fusion and transduction efficiency of primary CD34+ cells with human immunodeficiency virus 1-based lentiviral vectors reveal different effects of transduction enhancers, Hum. Gene Ther. Methods 25 (1) (2014) 48–56.
[8] D.L. Haas, S.S. Case, G.M. Crooks, D.B. Kohn, Critical factors influencing stable transduction of human CD34(+) cells with HIV-1-derived lentiviral vectors, Mol. Ther. 2 (1) (2000) 71–80.
[9] V. Sandrin, B. Boson, P. Salmon, W. Gay, D. Negre, R. Le Grand, D. Trono, F.L. Cosset, Lentiviral vectors pseudotyped with a modified RD114 envelope glycoprotein show increased stability in sera and augmented transduction of primary lymphocytes and CD34+ cells derived from human and nonhuman primates, Blood 100 (3) (2002) 823–832.
[10] C. Meier, T. Weil, F. Kirchhoff, J. Munch, Peptide nanofibrils as enhancers of retroviral gene transfer, Wiley Interdiscip. Rev. Nanomed. Nanobiotechnol. 6 (5) (2014) 438–451.
[11] F. Arnold, J. Schnell, O. Zirafi, C. Sturzel, C. Meier, T. Weil, L. Standker, W.G. Forssmann, N.R. Roan, W.C. Greene, F. Kirchhoff, J. Munch, Naturally occurring fragments from two distinct regions of the prostatic acid phosphatase form amyloidogenic enhancers of HIV infection, J. Virol. 86 (2) (2012) 1244–1249.
[12] J. Munch, E. Rucker, L. Standker, K. Adermann, C. Goffinet, M. Schindler, S. Wildum, R. Chinnadurai, D. Rajan, A. Specht, G. Gimenez-Gallego, P.C. Sanchez, D.M. Fowler, A. Koulov, J.W. Kelly, W. Mothes, J.C. Grivel, L. Margolis, O.T. Keppler, W.G. Forssmann, F. Kirchhoff, Semen-derived amyloid fibrils drastically enhance HIV infection, Cell 131 (6) (2007) 1059–1071.
[13] N.R. Roan, J.A. Muller, H. Liu, S. Chu, F. Arnold, C.M. Sturzel, P. Walther, M. Dong, H.E. Witkowska, F. Kirchhoff, J. Munch, W.C. Greene, Peptides released by physiological cleavage of semen coagulum proteins form amyloids that enhance HIV infection, Cell Host Microbe 10 (6) (2011) 541–550.
[14] M. Yolamanova, C. Meier, A.K. Shaytan, V. Vas, C.W. Bertoncini, F. Arnold, O. Zirafi, S.M. Usmani, J.A. Muller, D. Sauter, C. Goffinet, D. Palesch, P. Walther, N.R. Roan, H. Geiger, O. Lunov, T. Simmet, J. Bohne, H. Schrezenmeier, K. Schwarz, L. Standker, W.G. Forssmann, X. Salvatella, P.G. Khalatur, A.R. Khokhlov, T.P. Knowles, T. Weil, F. Kirchhoff, J. Munch, Peptide nanofibrils boost retroviral gene transfer and provide a rapid means for concentrating viruses, Nat. Nanotechnol. 8 (2) (2013) 130–136.
[15] L. Zhang, C. Jiang, H. Zhang, X. Gong, L. Yang, L. Miao, Y. Shi, Y. Zhang, W. Kong, C. Zhang, Y. Shan, A novel modified peptide derived from membrane-proximal external region of human immunodeficiency virus type 1 envelope significantly enhances retrovirus infection, J. Pept. Sci. 20 (1) (2014) 46–54.
[16] A. Kichler, C. Leborgne, J. Marz, O. Danos, B. Bechinger, Histidine-rich amphipathic peptide antibiotics promote efficient delivery of DNA into mammalian cells, Proc. Natl. Acad. Sci. U.S.A. 100 (4) (2003) 1564–1568.
[17] B. Bechinger, V. Vidovic, P. Bertani, A. Kichler, A new family of peptide-nucleic acid nanostructures with potent transfection activities, J. Pept. Sci. 17 (2) (2011) 88–93.
[18] A.J. Mason, C. Gasnier, A. Kichler, G. Prevost, D. Aunis, M.H. Metz-Boutigue, B. Bechinger, Enhanced membrane disruption and antibiotic action against pathogenic bacteria by designed histidine-rich peptides at acidic pH, Antimicrob. Agents Chemother. 50 (10) (2006) 3305–3311.
[19] A.J. Mason, A. Martinez, C. Glaubitz, O. Danos, A. Kichler, B. Bechinger, The antibiotic and DNA-transfecting peptide LAH4 selectively associates with, and disorders, anionic lipids in mixed membranes, FASEB J. 20 (2) (2006) 320–322.
[20] A. Marquette, A.J. Mason, B. Bechinger, Aggregation and membrane permeabilizing properties of designed histidine-containing cationic linear peptide antibiotics, J. Pept. Sci. 14 (4) (2008) 488–495.
[21] A.J. Mason, W. Moussaoui, T. Abdelrahman, A. Boukhari, P. Bertani, A. Marquette, P. Shooshtarizaheh, G. Moulay, N. Boehm, B. Guerold, R.J. Sawers, A. Kichler, M.H. Metz-Boutigue, E. Candolfi, G. Prevost, B. Bechinger, Structural determinants of antimicrobial and antiplasmodial activity and selectivity in histidine-rich amphipathic cationic peptides, J. Biol. Chem. 284 (1) (2009) 119–133.
[22] B. Langlet-Bertin, C. Leborgne, D. Scherman, B. Bechinger, A.J. Mason, A. Kichler, Design and evaluation of histidine-rich amphipathic peptides for siRNA delivery, Pharm. Res. 27 (7) (2010) 1426–1436.
[23] D. Fenard, S. Genries, D. Scherman, A. Galy, S. Martin, A. Kichler, Infectivity enhancement of different HIV-1-based lentiviral pseudotypes in presence of the cationic amphipathic peptide LAH4-L1, J. Virol. Methods 189 (2) (2013) 375–378.
[24] D. Fenard, D. Ingrao, A. Seye, J. Buisset, S. Genries, S. Martin, A. Kichler, A. Galy, Vectofusin-1, a new viral entry enhancer, strongly promotes lentiviral transduction of human hematopoietic stem cells, Mol. Ther. Nucl. Acids 2 (2013) e90.
[25] S. Majdoul, A.K. Seye, A. Kichler, N. Holic, A. Galy, B. Bechinger, D. Fenard, Molecular determinants of vectofusin-1 and its derivatives for the enhancement of lentivirally mediated gene transfer into hematopoietic stem/progenitor cells, J. Biol. Chem. 291 (5) (2016) 2161–2169.
[26] J.V. Fritz, P. Didier, J.P. Clamme, E. Schaub, D. Muriaux, C. Cabanne, N. Morellet, S. Bouaziz, J.L. Darlix, Y. Mely, H. de Rocquigny, Direct Vpr-Vpr interaction in cells monitored by two photon fluorescence correlation spectroscopy and fluorescence lifetime imaging, Retrovirology 5 (2008) 87.
[27] O.W. Merten, S. Charrier, N. Laroudie, S. Fauchille, C. Dugue, C. Jenny, M. Audit, M.A. Zanta-Boussif, H. Chautard, M. Radrizzani, G. Vallanti, L. Naldini, P.

Noguiez-Hellin, A. Galy, Large-scale manufacture and characterization of a lentiviral vector produced for clinical ex vivo gene therapy application, Hum. Gene Ther. 22 (3) (2011) 343–356.
[28] M.V. Sukhanova, S. Abrakhi, V. Joshi, D. Pastre, M.M. Kutuzov, R.O. Anarbaev, P.A. Curmi, L. Hamon, O.I. Lavrik, Single molecule detection of PARP1 and PARP2 interaction with DNA strand breaks and their poly(ADP-ribosyl)ation using high-resolution AFM imaging, Nucl. Acids Res. 44 (6) (2016) e60.
[29] S. Navea, R. Tauler, E. Goormaghtigh, A. de Juan, Chemometric tools for classification and elucidation of protein secondary structure from infrared and circular dichroism spectroscopic measurements, Proteins 63 (3) (2006) 527–541.
[30] N.R. Roan, J. Munch, N. Arhel, W. Mothes, J. Neidleman, A. Kobayashi, K. Smith-McCune, F. Kirchhoff, W.C. Greene, The cationic properties of SEVI underlie its ability to enhance human immunodeficiency virus infection, J. Virol. 83 (1) (2009) 73–80.
[31] V. Iacobucci, F. Di Giuseppe, T.T. Bui, L.S. Vermeer, J. Patel, D. Scherman, A. Kichler, A.F. Drake, A.J. Mason, Control of pH responsive peptide self-association during endocytosis is required for effective gene transfer, Biochim. Biophys. Acta 1818 (5) (2012) 1332–1341.
[32] Y. Lan, B. Langlet-Bertin, V. Abbate, L.S. Vermeer, X.L. Kong, K.E. Sullivan, C. Leborgne, D. Scherman, R.C. Hider, A.F. Drake, S.S. Bansal, A. Kichler, A.J. Mason, Incorporation of 2,3-diaminopropionic acid into linear cationic amphipathic peptides produces ph-sensitive vectors, Chembiochem 11 (9) (2010) 1266–1272.
[33] V. Abbate, W. Liang, J. Patel, Y. Lan, L. Capriotti, V. Iacobucci, T.T. Bui, P. Chaudhuri, L. Kudsiova, L.S. Vermeer, P.F. Chan, X. Kong, A.F. Drake, J.K. Lam, S.S. Bansal, A.J. Mason, Manipulating the pH response of 2,3-diaminopropionic acid rich peptides to mediate highly effective gene silencing with low-toxicity, J. Control. Release 172 (3) (2013) 929–938.
[34] N.E. Zhou, C.M. Kay, R.S. Hodges, Synthetic model proteins: the relative contribution of leucine residues at the nonequivalent positions of the 3–4 hydrophobic repeat to the stability of the two-stranded alpha-helical coiled-coil, Biochemistry 31 (25) (1992) 5739–5746.
[35] N. Nespovitaya, J. Gath, K. Barylyuk, C. Seuring, B.H. Meier, R. Riek, Dynamic assembly and disassembly of functional beta-endorphin amyloid fibrils, J. Am. Chem. Soc. 138 (3) (2016) 846–856.
[36] X.Y. Jin, L. Leclercq, N. Sisavath, H. Cottet, Investigating the influence of phosphate ions on poly(L-lysine) conformations by Taylor dispersion analysis, Macromolecules 47 (15) (2014) 5320–5327.
[37] R.M. Verly, J.M. Resende, E.F.C. Junior, M.T.Q. de Magalhães, C.F.C.R. Guimarães, V.H.O. Munhoz, M.P. Bemquerer, F.C.L. Almeida, M.M. Santoro, D. Piló-Veloso, B. Bechinger, Structure and membrane interactions of the homodimeric antibiotic peptide homotarsinin, Sci. Rep. 7 (2017) 40854.
[38] F. Chiti, P. Webster, N. Taddei, A. Clark, M. Stefani, G. Ramponi, C.M. Dobson, Designing conditions for in vitro formation of amyloid protofilaments and fibrils, Proc. Natl. Acad. Sci. U.S.A. 96 (7) (1999) 3590–3594.
[39] H. Dong, S.E. Paramonov, J.D. Hartgerink, Self-assembly of alpha-helical coiled coil nanofibers, J. Am. Chem. Soc. 130 (41) (2008) 13691–13695.
[40] A. Barth, Infrared spectroscopy of proteins, Biochim. Biophys. Acta 1767 (9) (2007) 1073–1101.
[41] R. Khurana, C. Coleman, C. Ionescu-Zanetti, S.A. Carter, V. Krishna, R.K. Grover, R. Roy, S. Singh, Mechanism of thioflavin T binding to amyloid fibrils, J. Struct. Biol. 151 (3) (2005) 229–238.
[42] K.A. Burke, E.A. Yates, J. Legleiter, Biophysical insights into how surfaces, including lipid membranes, modulate protein aggregation related to neurodegeneration, Front. Neurol. 4 (2013) 17.
[43] R. Kayed, A. Pensalfini, L. Margol, Y. Sokolov, F. Sarsoza, E. Head, J. Hall, C. Glabe, Annular protofibrils are a structurally and functionally distinct type of amyloid oligomer, J. Biol. Chem. 284 (7) (2009) 4230–4237.
[44] H.A. Lashuel, D. Hartley, B.M. Petre, T. Walz, P.T. Lansbury Jr., Neurodegenerative disease: amyloid pores from pathogenic mutations, Nature 418 (6895) (2002) 291.
[45] M. Zhu, S. Han, F. Zhou, S.A. Carter, A.L. Fink, Annular oligomeric amyloid intermediates observed by in situ atomic force microscopy, J. Biol. Chem. 279 (23) (2004) 24452–24459.
[46] B. Apostolovic, M. Danial, H.A. Klok, Coiled coils: attractive protein folding motifs for the fabrication of self-assembled, responsive and bioactive materials, Chem. Soc. Rev. 39 (9) (2010) 3541–3575.
[47] J.M. Mason, K.M. Arndt, Coiled coil domains: stability, specificity, and biological implications, Chembiochem 5 (2) (2004) 170–176.
[48] K. Beck, B. Brodsky, Supercoiled protein motifs: the collagen triple-helix and the alpha-helical coiled coil, J. Struct. Biol. 122 (1–2) (1998) 17–29.
[49] B. Bechinger, Insights into the mechanisms of action of host defence peptides from biophysical and structural investigations, J. Pept. Sci. 17 (5) (2011) 306–314.
[50] S. Mondal, E. Gazit, The self-assembly of helical peptide building blocks, ChemNanoMat 2 (5) (2016) 323–332.
[51] Y. Wu, J.H. Collier, alpha-Helical coiled-coil peptide materials for biomedical applications, Wiley Interdiscip. Rev. Nanomed. Nanobiotechnol. (2016).
[52] C. Xu, R. Liu, A.K. Mehta, R.C. Guerrero-Ferreira, E.R. Wright, S. Dunin-Horkawicz, K. Morris, L.C. Serpell, X. Zuo, J.S. Wall, V.P. Conticello, Rational design of helical nanotubes from self-assembly of coiled-coil lock washers, J. Am. Chem. Soc. 135 (41) (2013) 15565–15578.
[53] S. Kojima, Y. Kuriki, T. Yoshida, K. Yazaki, K. Miura, Fibril formation by an amphipathic alpha-helix-forming polypeptide produced by gene engineering, Proc. Jpn. Acad. Ser. B-Phys. Biol. Sci. 73 (1) (1997) 7–11.
[54] S.A. Potekhin, T.N. Melnik, V. Popov, N.F. Lanina, A.A. Vazina, P. Rigler, A.S. Verdini, G. Corradin, A.V. Kajava, De novo design of fibrils made of short alpha-helical coiled coil peptides, Chem. Biol. 8 (11) (2001) 1025–1032.
[55] M.J. Pandya, G.M. Spooner, M. Sunde, J.R. Thorpe, A. Rodger, D.N. Woolfson, Sticky-end assembly of a designed peptide fiber provides insight into protein fibrillogenesis, Biochemistry 39 (30) (2000) 8728–8734.
[56] E.F. Banwell, E.S. Abelardo, D.J. Adams, M.A. Birchall, A. Corrigan, A.M. Donald, M. Kirkland, L.C. Serpell, M.F. Butler, D.N. Woolfson, Rational design and application of responsive alpha-helical peptide hydrogels, Nat. Mater. 8 (7) (2009) 596–600.
[57] C. Loudet, L. Khemtemourian, F. Aussenac, S. Gineste, M.F. Achard, E.J. Dufourc, Bicelle membranes and their use for hydrophobic peptide studies by circular dichroism and solid state NMR, Biochim. Biophys. Acta 1724 (3) (2005) 315–323.
[58] J. Heyda, P.E. Mason, P. Jungwirth, Attractive interactions between side chains of histidine-histidine and histidine-arginine-based cationic dipeptides in water, J. Phys. Chem. B 114 (26) (2010) 8744–8749.
[59] S.M. Liao, Q.S. Du, J.Z. Meng, Z.W. Pang, R.B. Huang, The multiple roles of histidine in protein interactions, Chem. Cent. J. 7 (1) (2013) 44.
[60] L.S. Vermeer, Y. Lan, V. Abbate, E. Ruh, T.T. Bui, L.J. Wilkinson, T. Kanno, E. Jumagulova, J. Kozlowska, J. Patel, C.A. McIntyre, W.C. Yam, G. Siu, R.A. Atkinson, J.K. Lam, S.S. Bansal, A.F. Drake, G.H. Mitchell, A.J. Mason, Conformational flexibility determines selectivity and antibacterial, antiplasmodial, and anticancer potency of cationic alpha-helical peptides, J. Biol. Chem. 287 (41) (2012) 34120–34133.
[61] J. Georgescu, V.H. Munhoz, B. Bechinger, NMR structures of the histidine-rich peptide LAH4 in micellar environments: membrane insertion, pH-dependent mode of antimicrobial action, and DNA transfection, Biophys. J. 99 (8) (2010) 2507–2515.
[62] T.P. Knowles, M. Vendruscolo, C.M. Dobson, The amyloid state and its association with protein misfolding diseases, Nat. Rev. Mol. Cell. Biol. 15 (6) (2014) 384–396.